Journal of Physiology (1988), **399**, *pp.* 493–517
With 11 *text-figures*
Printed in Great Britain

CHARACTERIZATION OF VOLTAGE-GATED SODIUM CHANNELS IN OVINE GONADOTROPHS: RELATIONSHIP TO HORMONE SECRETION

BY W. T. MASON AND S. K. SIKDAR

From the Department of Neuroendocrinology, AFRC Institute of Animal Physiology and Genetics Research, Babraham, Cambridge CB2 4AT

(*Received 27 April 1987*)

SUMMARY

1. The properties of whole-cell Na^+ currents (I_{Na}) were studied in immunocytochemically identified ovine gonadotrophs using the patch clamp technique.

2. Voltage recording under current clamp revealed that gonadotrophs did not fire spontaneously, and fired only a single action potential in response to a depolarizing current clamp step.

3. Under voltage clamp, I_{Na} was found to be sensitive to tetrodotoxin (TTX) and had an activation threshold of about -75 mV, with peak current occurring at -20 to -30 mV.

4. Using a two-pulse protocol a delay in the onset of inactivation was observed, suggesting that inactivation is dependent on and preceded by the activation phenomenon.

5. Kinetics of recovery from inactivation of the Na^+ channels were studied with test pulses applied at various times after a depolarizing pre-pulse. Recovery from inactivation showed an initial delay, in contrast to the predictions of the Hodgkin–Huxley equations.

6. Recovery from inactivation was examined by using a repetitive pulse protocol, showing approximately 1 s is required for the channels to achieve a 95% recovery.

7. The steady-state inactivation (h_∞–V) curve was sigmoidal and fitted by a logistic growth curve model. The half-inactivation value of the Na^+ current occurred at a membrane potential of -70 ± 8 mV.

8. Noise power spectra derived from fluctuations of I_{Na} could be fitted with a single Lorentzian function, and the time constant value was slower at more depolarizing potentials.

9. The single-Na^+-channel conductance was estimated from fluctuation analysis under conditions of reduced Na^+ current amplitude by depolarizing pre-pulses. The single-channel conductance derived by the above method ($\simeq$ 11 pS) corresponded to the single-channel conductance derived from single-channel current measurements using the outside-out version of the patch clamp technique ($\simeq$ 13 pS).

10. Inactivation of I_{Na} was slowed by including 15 mM-iodate in the pipette. Ensemble fluctuation analysis of I_{Na} under these conditions was carried out using the steady-state portion of the inactivation phase of the modified I_{Na} records, revealing a process best fitted by a double Lorentzian power spectrum, consistent with

inactivation kinetics involving both a fast and a slow process. The time constant values correlated well with those obtained from a double-exponential fit to the decaying inactivation phase of the iodate-modified I_{Na}.

11. From the analysis of gonadotroph I_{Na} kinetics, the activation and inactivation of the channels governing the opening and closing of the channels to a voltage pulse is best described by a coupled-reaction model, with one open state intermediate between a closed state and two inactivated states.

12. The results are discussed in relation to the fact that LH secretion does not appear to be dependent on the activity of voltage-activated I_{Na}, since it is unaffected by TTX blockade or removal of Na^+ from the extracellular space.

INTRODUCTION

The role of gonadotrophs in the control and maintenance of reproduction is an important one, since the cells secrete the reproductive hormones, luteinizing hormone (LH) and follicle stimulating hormone (FSH) under the influence of the hypothalamic decapeptide, gonadotrophin releasing hormone (GNRH).

The electrical properties of gonadotrophin-secreting cells have not been studied due to the variety of different cell types found in the anterior pituitary and difficulty in selectively isolating the gonadotrophs (Denef, Swennen & Andries, 1982; Childs, Hyde, Naor & Catt, 1983). However, the discovery that the ovine pars tuberalis contains gonadotrophs as the only hormone-secreting cell type (Gross, Turgeon & Waring, 1984) has made possible the isolation and long-term culture of a pure population of gonadotrophs (Mason & Waring, 1985, 1986). These cells are similar to those of the pars distalis in immunocytochemical staining for LH, and have functionally identical responses to GNRH and steroids (Gross, 1978; Agnado, Hancke, Rodriguez & Rodriguez, 1982; Gross *et al.* 1984).

The mechanism of regulation of pituitary hormone secretion has been suggested to involve changes in the membrane potential and action potential frequency (Kidokoro, 1976; Tareskevich & Douglas, 1977). Sodium channels are ubiquitous in excitable neuronal cells, with many features in common, and because the kinetics of voltage-gated ionic channels control membrane excitability, it is important that knowledge of these kinetics is obtained, allowing assessment of their importance in hormone secretion. Subtle differences in channel kinetics might give some insight into the importance of voltage-activated membrane phenomena in non-neuronal cells.

This article has analysed voltage gated Na^+ channels in ovine gonadotrophs using the whole-cell recording mode of the patch clamp technique (Hamill, Marty, Neher, Sakmann & Sigworth, 1981). While most of the study pertains to the details of gating kinetics of Na^+ channels, we have also attempted to relate the observations on aspects of Na^+ channel kinetics to GNRH-mediated hormone release of LH by these cells under physiological conditions.

Part of the work has been presented previously (Mason, Sikdar & Waring, 1986) in the form of a communication to the Physiological Society.

METHODS

Cell preparation

Gonadotrophs were isolated, dispersed and cultured from the ovine pars tuberalis as described previously (Mason & Waring, 1985, 1986).

Recording procedures

Recordings were made from isolated gonadotrophs using the methods of Hamill *et al.* (1981). Electrodes were pulled from Pyrex tubing (1·2 mm o.d., Clarke Electromedical) and had resistances in the range of 2–8 MΩ. The electrode was connected to a patch clamp amplifier (List Electronic, F.R.G., L/M EPC-7), earthed to the bath by a Ag–AgCl bridge. For whole-cell recording, initial compensation of the capacitance and series resistance was made by setting the G-series (series conductance), C-slow (cell capacitance), C-fast (pipette and stray capacitance) and percentage compensation to appropriate levels to cause minimal distortion of the capacitive current traces. Series resistances measured following compensation were in the range of 2–8 MΩ.

The cell capacitance (C_m) was estimated from the relation $\tau = R_m C_m$, by passing a 500 ms hyperpolarizing current pulse, where τ is the time constant of the voltage deflection to reach the steady-state value, derived from a single-exponential fit of the curve and R_m is the input resistance of the cell. Estimated cell capacitance fell in the range of 8–19 pF (mean ± S.D. = 12·58 ± 3·75 pF, $n = 8$). Voltage and current recordings were led through a Sony PCM 701ES encoder/decoder and stored on magnetic tape using a Sony video recorder which had a recording bandwidth of 16 kHz.

Data analaysis

Data analysis was performed off-line by prior filtering (1–4 kHz) and digitizing (8 kHz) using a PDP 11/73 computer interfaced with a Cambridge Electronic Design interface (CED 502), stored on a Winchester hard disc. The ANADISK and DA23 library of programs provided by T. D. Lamb (1983) were utilized for data acquisition, and capacitance–leakage subtraction. Single-current waveforms were captured for curve-fitting analysis using the SAQ5 software (Mr J. Dempster, University of Strathclyde), with sampling frequencies in excess of 20 kHz.

The sodium current (I_{Na}) decay after peak activation and the tail current decay were fitted with either a single-exponential function of the form

$$I_{Na}t = I'_{Na} \exp(-t/\tau_1), \tag{1}$$

or a double-exponential function of the form

$$I_{Na}t = I'_{Na} \exp(-t/\tau_1) + I'_{Na} \exp(-t/\tau_2), \tag{2}$$

where I'_{Na} and I'_{Na} are amplitudes, t is time, and τ_1 and τ_2 are time constants of fast and slow processes respectively. An iterative least-squares minimizing curve fit of the exponential functions (eqns (1) and (2)) on averaged data was performed using the programs provided by J. D. Dempster (University of Strathclyde).

The power density spectra were fitted either by Lorentzian functions of the form

$$S(f) = S(0)/[1 + (2\pi f\tau_1)^2], \tag{3}$$

or a double-Lorentzian function

$$S(f) = S(0)/\{[1 + (2\pi f\tau_1)^2] + [1 + (2\pi f\tau_2)^2]\}, \tag{4}$$

where f is frequency in hertz and $S(0)$ is the spectral density at 0 Hz.

A maximum likelihood program (MLP) data analysis package running on a local VAX Agrenet network was used to fit Lorentzian functions. Linear regression analysis was performed using the Minitab software package.

Similarly, fits of the logistic growth curve model for sigmoidal curve fitting of the form given below were performed utilizing the MLP package

$$y = 1/\{1 + \exp[(V - V'_h)/k]\}, \tag{5}$$

where V'_h is the potential for half-maximal current and k is the slope factor.

Solutions

For recording purposes the culture dish was mounted on the stage of an inverted microscope with phase-contrast optics (Leitz). The compositions of the solutions are listed in Table 1. All chemicals were from Sigma. After three or four quick rinses with the test solutions the culture dish was filled with a total volume of 1 ml test solution. Tetrodotoxin (TTX, 1–20 μM) was applied directly to the bath.

Hormone release

Cells from the pars distalis were collagenase dispersed and plated in 24-well plates (Nunc) at a density of 1×10^5 cells/well (Mason & Waring, 1985). Following 2 days of incubation in Dulbecco's modified Eagle's medium (DMEM with L-valine), the medium was removed and the cells incubated for 2 h with a solution containing (mM): NaCl, 127; KCl, 5; $MgCl_2$, 2; $CaCl_2$, 5; NaH_2PO_4, 1; $NaHCO_3$, 5; HEPES, 10; glucose, 10; pH 7·4. Following this incubation, the medium was changed to one containing the test substances. Isotonic choline chloride was used to replace Na^+ in the Na^+-free solution ($-Na^+$). The medium was removed 2 h later and LH assayed by radioimmunoassay using a rabbit antiserum to ovine LH prepared locally against NIH ovine-S18, with an NIH pituitary program sample (NIH-LH-S18) of ovine LH as the standard.

TABLE 1. Composition of solutions (mM)

	NaCl	KCl	$CaCl_2$	HEPES	Glucose	EGTA	TEA-Cl	CsCl	$NaIO_3$
Control soln	135	5	—	5	10	—	—	—	—
Na^+ soln	135	—	—	5	10	—	10	—	—
K^+ soln	—	130	1	5	10	10	—	—	—
Cs^+ soln	5	—	1	5	10	10	—	125	—
IO_3^- soln	—	—	1	5	10	10	—	115	15

RESULTS

Identification of the sodium current

With mixed Na^+ and K^+ as the control external solutions, the gonadotrophs responded to depolarizing current pulses with a single spike-like depolarizing event resembling an action potential. Increasing the amplitude of the current pulse reduced the latency of firing, but did not elicit multiple depolarizing events in the majority of cells examined (93%, $n = 27$).

The steady-state voltage deflections (following the initial depolarizing event) were symmetrical to identical depolarizing and hyperpolarizing current, indicating little

Fig. 1. *A* and *B*, identification of voltage-gated Na^+ channels using 10 μM-TTX in gonadotrophs isolated from sheep pars tuberalis. *A*, voltage responses of a gonadotroph to depolarizing and hyperpolarizing current steps recorded with the patch clamp technique in the whole-cell recording mode under current clamp. Membrane potential (V_m) maintained at -90 mV by DC injection. The pipette was filled with K^+-rich internal solution to dialyse the cells and the external bath medium contained control solution. The short and sharp rising depolarizing event evoked by depolarizing current pulses in control (*a*) was aborted on addition of 10 μM-TTX to the bath medium (*b*). *B*, mixed inward and outward current responses in the same cell in voltage clamp. Control (*a*) and in the presence of 10 μM-TTX in the bath medium (*b*). Note the specific blockade of the inward current by TTX. *C*, isolated Na^+ currents. *a*, averaged Na^+ current records ($n = 5$) obtained by a 40 ms depolarization step to membrane potentials indicated on the left starting from a holding potential (V_h) of -100 mV. *b*, plot of peak I_{Na} obtained from the same cell shown in *a* against the membrane potential.

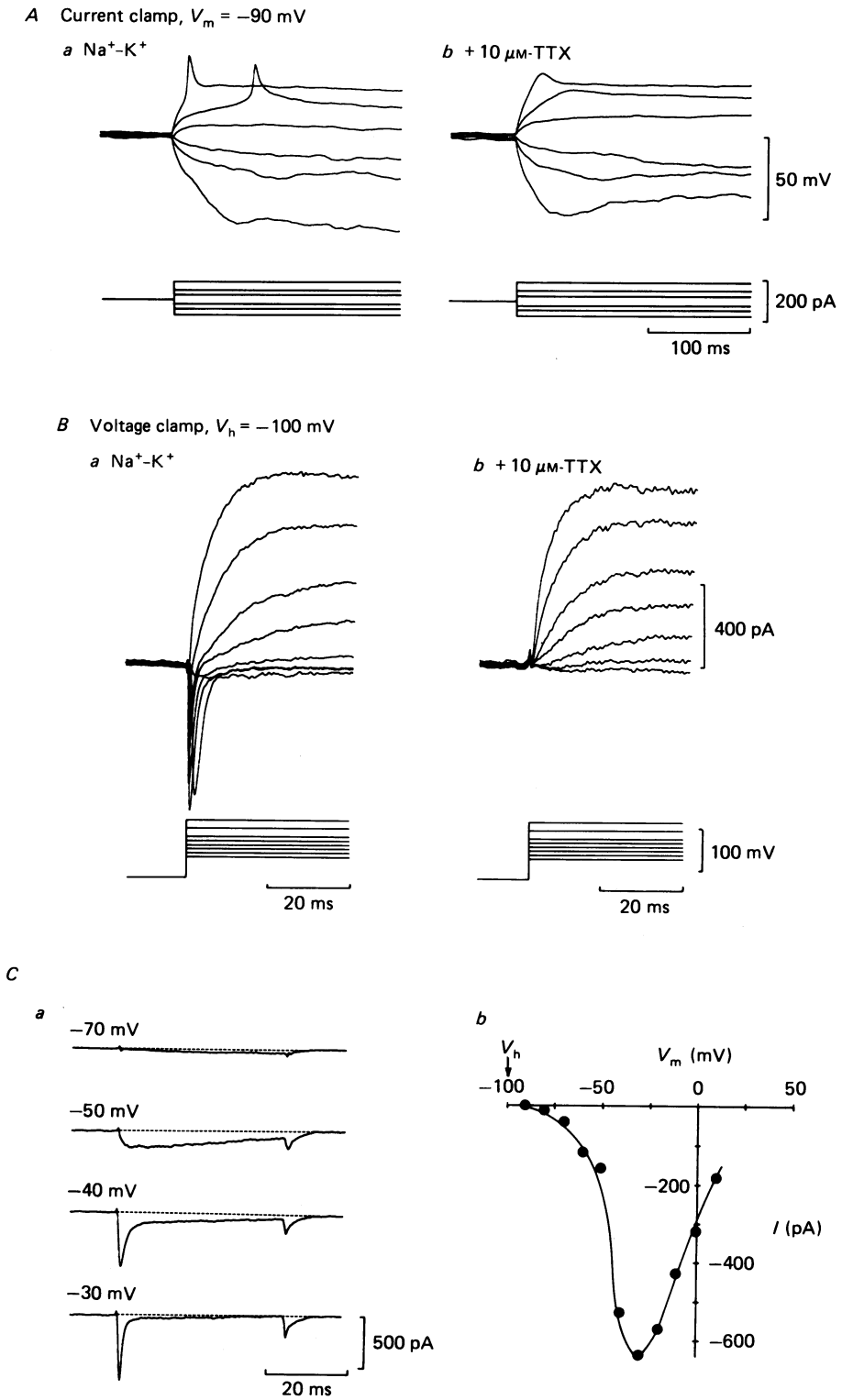

Fig. 1. For legend see opposite.

rectification in the I–V relationship. Tetrodotoxin (10 μM) reduced the amplitude of the initial depolarizing event recorded in the external solution of mixed ionic composition, K^+, Control soln, Table 1 (Fig. 1*A*).

Under voltage clamp in the same cells, the current traces showed mixed inward and outward currents. Addition of TTX produced block of the inward component (Fig. 1*B*), whereas the outward currents were attenuated by tetraethylammonium chloride (TEA, 10 mM).

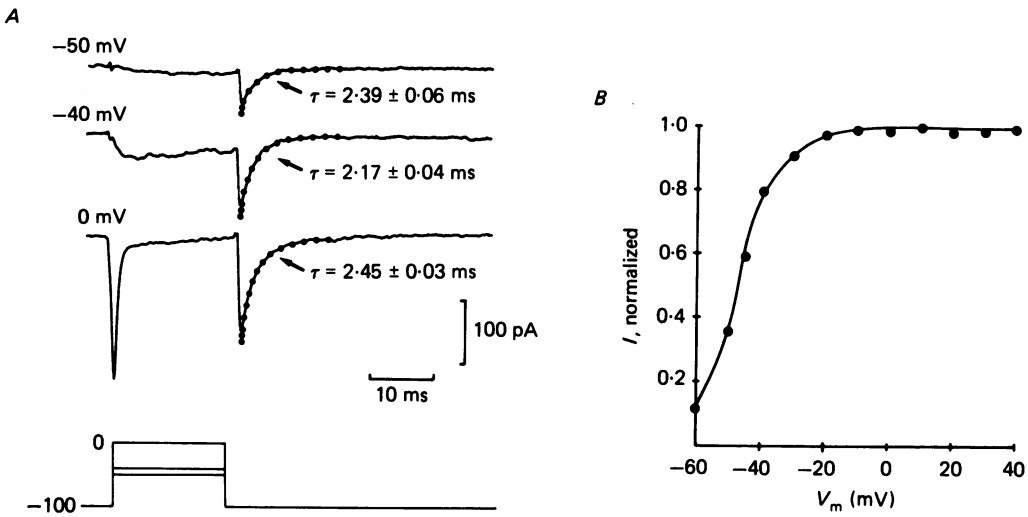

Fig. 2. Sodium tail current at different test potentials. *A*, Na^+ inward and tail currents produced at the membrane potentials indicated on the left of the traces, using a depolarizing voltage step from a holding potential of −100 mV. The dots superimposed on the tail current decay signify a monoexponential fit (eqn (1)). The initial 2 ms of the tail current traces were discarded to remove contaminating capacitive transients. The time constants derived from the monoexponential fits are indicated on the traces. Note the close similarity in the time constant values. *B*, plot of the normalized (with respect to the maximal tail current) tail current amplitude against membrane potential (V_m). The Na^+ tail current amplitudes were determined from the exponential fits by extrapolation to the end of the pulse. The tail current amplitudes have been normalized relative to the maximal tail current amplitude. The line was fitted by eqn (5) in the text for a logistic growth curve model. The half-activation value (V_h in eqn (5) was −49 mV, with a slope factor (k) of 10 mV.

Isolated sodium current

Voltage-activated Na^+ currents were examined after dialysing the cells with K^+-free, Cs^+-containing solution (Cs^+ soln, Table 1), while the bath contained Ca^{2+}- and K^+-free Na^+ solution (Na^+ soln, Table 1). Figure 1*Ca* depicts the isolated inward I_{Na} records with rapid activation–inactivation characteristics at different membrane potentials and I_{Na} tail current relaxations on returning the test pulse to the holding potential level. An I–V plot of the peak I_{Na} amplitudes at different membrane potentials indicated the peak activation of I_{Na} to occur at between −20 and −30 mV (Fig. 1*Cb*). The maximal amplitude of I_{Na} varied between cells from 0·15 to 1·3 nA (n = 53).

Sodium tail current at different test potentials

Figure 2 shows the I_{Na} and the tail currents following step depolarizations, from a holding potential of -100 mV. The tail currents (produced at the end of the test pulse due to a sudden change in the driving force), were TTX sensitive and could be approximated by a single-exponential function (eqn (1)) extrapolated to the end of the pulse. Tail current amplitude was obtained by extrapolation to the end of the pulse. Tail current decay time constants for different test pulse amplitudes were similar (Fig. 2*A*), which indicates that the deactivation time constants were independent of the activating potential. Figure 2*B* is a plot of membrane potential *versus* the normalized tail current amplitude. A sigmoidal relationship was revealed by saturation occurring at more depolarized potentials, indicative of saturation in the Na^+ conductance. This could also be related to the activation kinetics of the Na^+ channels, with the half-maximal activation occurring at about -49 mV, derived from the logistic growth model fitted (eqn (5)) to the data points in Fig. 2*B*.

Inactivation of I_{Na} tail currents at different pulse durations

Since the magnitude of tail currents following activation of I_{Na} is proportional to the activatable fraction of Na^+ channels, the tail current method was used to examine Na^+ channel behaviour during the inactivation phase of I_{Na} (Fig. 3*A*). Tail current amplitude was maximal at a test pulse duration producing near maximal activation of I_{Na} (Fig. 3*Aa*). The inactivation phase set in with increasing pulse duration indicated by a decline in I_{Na} and accompanied by a reduction in the tail current amplitudes (Fig. 3*Ab–d*).

The tail current decay which parallels I_{Na} decay indicates a decline in the number of activatable Na^+ channels. This suggests that I_{Na} inactivation is due to a decrease in I_{Na} and not to simultaneous activation of outward current. The inactivation phase of the macroscopic I_{Na} can therefore be explained by changes in the gating kinetics of the open Na^+ channels which, once maximally activated, are mobilized to close.

Steady-state inactivation

The steady-state inactivation (h_∞) was measured by observing the I_{Na} amplitude produced to a standard test pulse to elicit maximal inward Na^+ current (judged from an I–V relationship) at different holding potentials. A plot of normalized peak I_{Na} and plotted against holding potential gave the h_∞–V plot. For the cell shown in Fig. 3*B* the membrane potential at which half-maximal steady-state inactivation occurred was -74 mV (V_h' in eqn (5)). This value falls near the resting membrane potential (-69 ± 7 mV, mean $\pm$ S.D., $n = 27$), and indicates that only about 50% of the gonadotroph Na^+ channels are available for activation at rest. The slope factor k was 3·6 mV.

Inactivation time constant

The inactivating component of I_{Na} decayed exponentially and the time constant of the early phase of I_{Na} inactivation was obtained by fitting eqn (1) to I_{Na} after peak values.

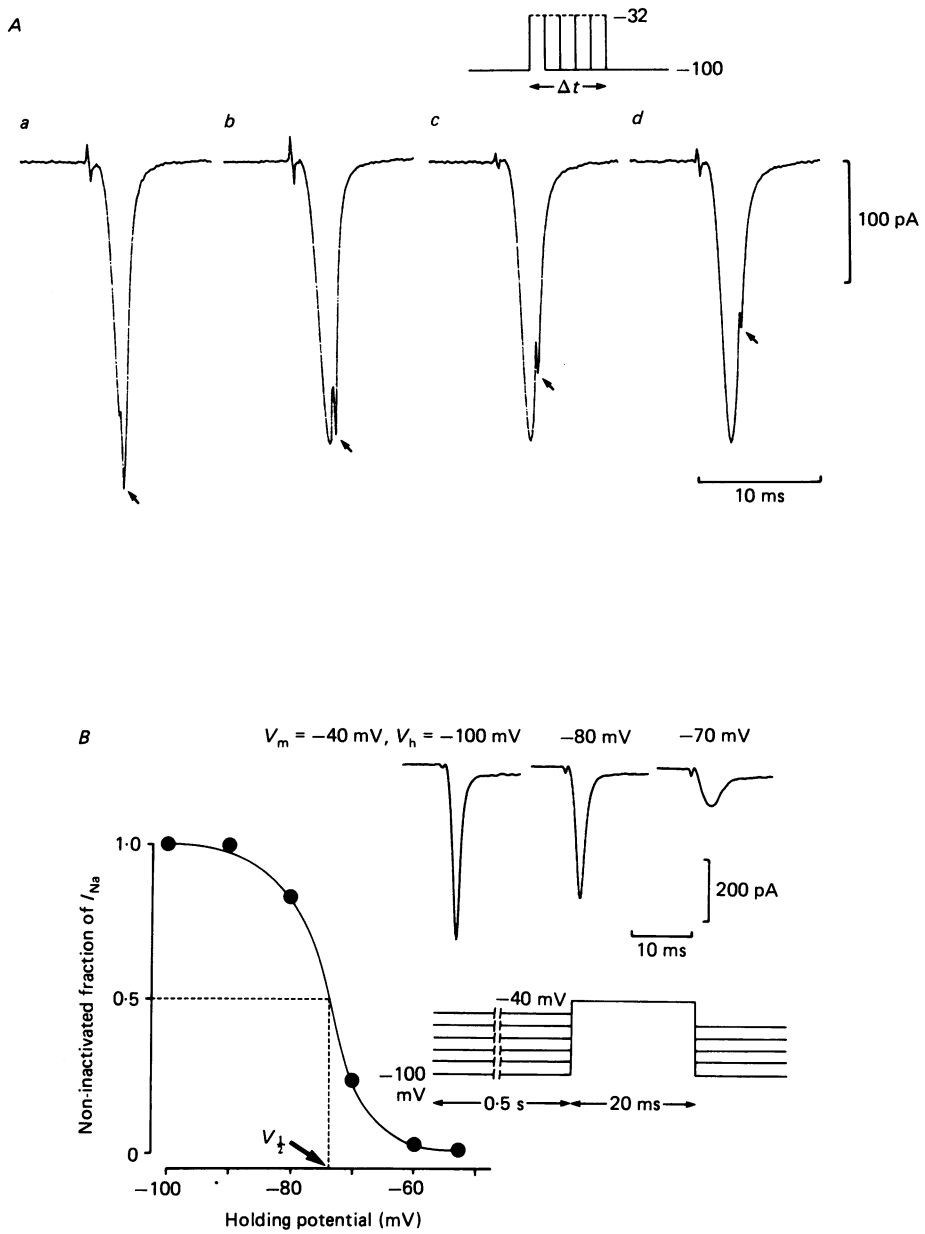

Fig. 3. *A*, Tail currents at different pulse durations. The arrows indicate the tail currents. The membrane potential was raised to −32 mV from a holding potential of −100 mV. *B*, voltage dependence of steady-state inactivation variable (h_∞) for gonadotroph Na^+ current. The inset shows the peak Na^+ current amplitudes produced on raising the membrane potential (V_m) to −40 mV from different holding potential levels (V_h) indicated above the traces. The graph is an h_∞–V plot obtained by plotting the non-inactivated fraction of the peak Na^+ current normalized with respect to the maximal current amplitude against the holding potential. The line was drawn according to eqn (5) in the text for a logistic growth model curve. The half-inactivation value ($V_{\frac{1}{2}}$ or V'_h in eqn (5)) was −74 mV, with a slope factor (k) of 3·6 mV.

The time constant of inactivation (τ_h) was voltage dependent. For the cell shown in Fig. 4, τ_h was about 0·87 ms at a membrane potential of −40 mV and 0·72 ms at −20 mV (Fig. 4*A*). The inactivation time constant decreased with increasing depolarization (Fig. 4*B*).

Lag in the onset of inactivation

To examine whether the inactivation phase of I_{Na} was dependent on activation, we employed a two-pulse protocol. A conditioning pulse to −30 mV of variable duration (in 100 μs increments) was followed without delay by a test pulse to −20 mV of 10 ms duration. The assumption was that the peak current amplitude produced by the test pulse represents the fraction of Na^+ channels activatable at the end of the conditioning pulse.

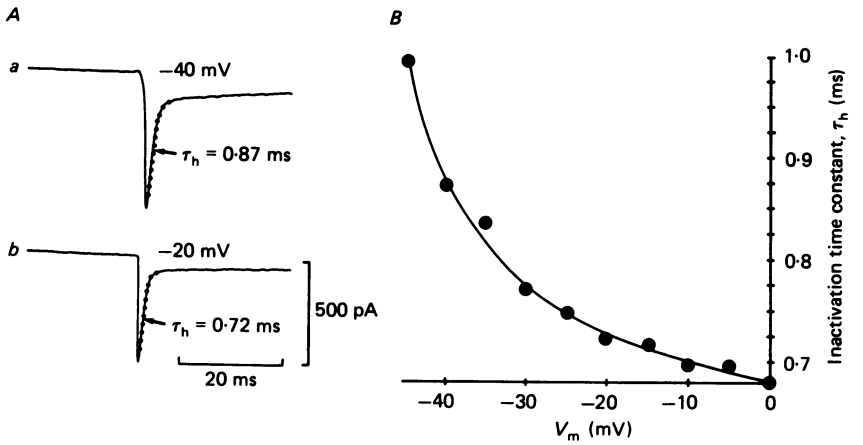

Fig. 4. Voltage dependence of inactivation time constant. *A*, Na^+ current inactivation at two different membrane potentials showing the Na^+ current decays. Averaged Na^+ current records (n = 10) at two different membrane potentials indicated above the traces. The dots on the inactivation phase of Na^+ currents signify fitting by the monoexponential function (eqn (1) in the text). The inactivation time constant at less depolarized potentials was slower (τ_h = 0·87 ms, −40 mV), than at a more depolarized potential (0·7 ms, −20 mV). *B*, plot of the inactivation time constant derived from the monoexponential fit of the inactivation phase against the membrane potential.

An initial delay of 700 μs in the onset of inactivation was revealed. This is demonstrated by similar current amplitudes (●, Fig. 5*A*) to the test pulse in the absence (0 ms) and following a 0·5 ms conditioning pulse. Further increments in conditioning pulse duration caused progressive decline of the test current (Fig. 5*A*). This suggests that activation must proceed before inactivation can develop.

Recovery of the sodium current

Recovery of I_{Na} following inactivation was studied with test pulses applied at different delay times after a conditioning pulse of similar amplitude (membrane potential, −20 mV). Recovery occurred during the interpulse interval at the holding potential of the cell (−100 mV). Figure 5*Ba*, shows the amplitudes of the peak I_{Na} at two different time delays following a conditioning pulse. By superimposing the

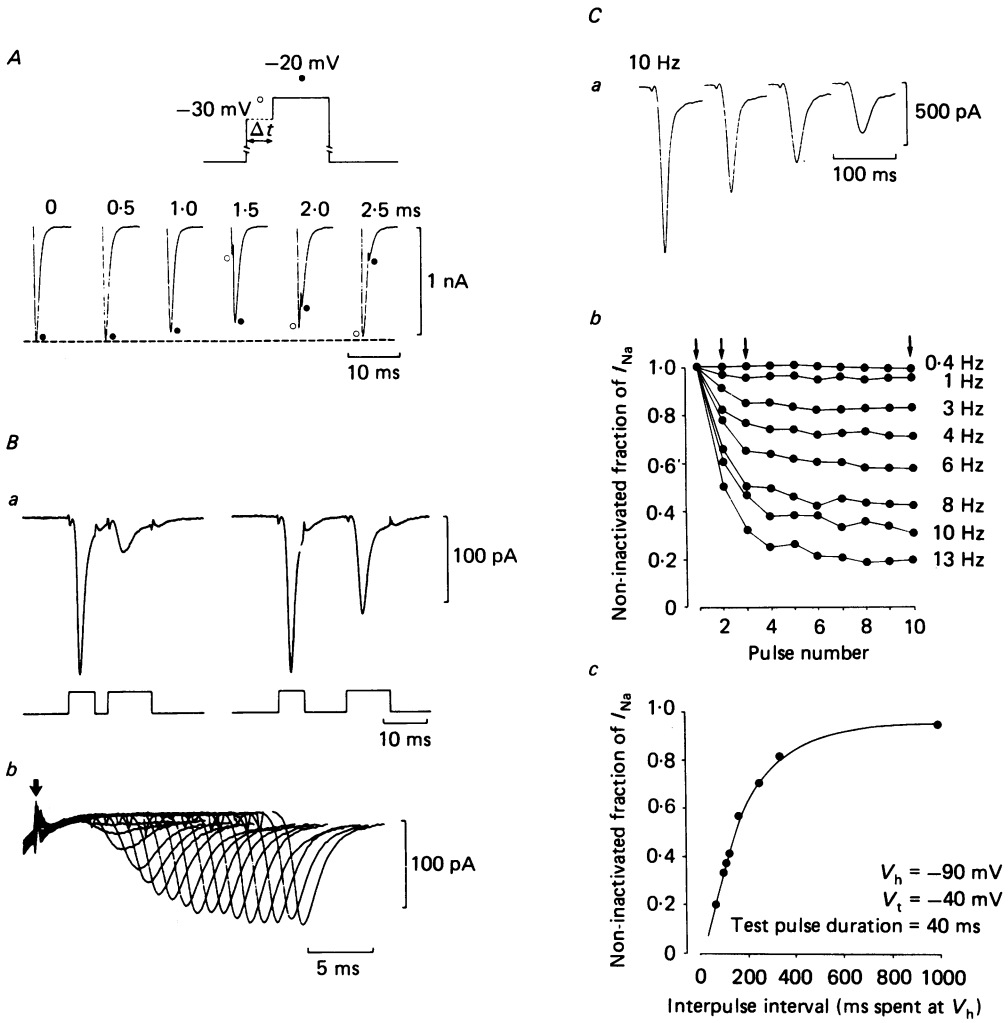

Fig. 5. *A*, delay in the onset of inactivation. A two-pulse protocol without gap in between was used. The duration of the conditioning pulse was varied in 100 μs steps, and only the currents to the conditioning (V_m = −30 mV; current, ○) and test pulses (V_m = −20 mV; current, ●) are plotted sequentially following 500 μs increments of the test pulse duration. Note the rapid decline in the test current amplitude following the development of the current to the conditioning pulse. *B*, delay in recovery from inactivation. *a*, two-pulse method to assess degree of recovery from inactivation. Upper trace, current; lower trace, voltage protocol. Sodium channels were inactivated by a 5 ms pre-pulse to −20 mV from a holding potential of −100 mV, and subsequently followed by a second pulse to the same potential as the pre-pulse for a similar duration. The size of Na^+ current produced by the second pulse following two different recovery intervals reflects the degree of recovery from previous inactivation. In *b*, the arrow marks the termination of the pre-pulse and repolarization to the holding potential of −100 mV, and the current trace to the left of the arrow is the last portion of the current produced by the pre-pulse. The current traces on the right of the arrow mark superimposed averaged test currents (n = 10) produced by applying a test pulse at various times after the pre-pulse. The superimposed test currents show the sigmoidal time course of recovery. Note the delay of about 4 ms in the onset of recovery. *C*, frequency dependence of recovery from I_{Na}

test currents produced by a sequence of test pulses applied at different times after the conditioning pulse, the amplitude of peak I_{Na} indicated the time course of recovery (Fig. 5*Bb*). Following an initial delay, the recovery of I_{Na} showed a sigmoidal time course.

Frequency dependence of reactivation following inactivation of the sodium current

A repetitive pulse protocol at different frequencies was used to analyse the time dependence of reactivation. Figure 5*Ca* and *b* show that the amplitude of I_{Na} decreases during the train with a constant interpulse interval. At higher frequencies, the decrease in I_{Na} occurs much earlier during the train and reaches a steady state. The I_{Na} amplitude at the equilibrated state (normalized with respect to I_{Na} produced by the first pulse in the train) was utilized to plot the reactivation of I_{Na} (Fig. 5*Cc*): this represents a quantitative measure of Na^+ channel behaviour to repeated activation. From this plot, 95% recovery of I_{Na} requires 1 s following activation.

Characteristics of sodium tail currents at different repolarization potentials

The kinetics of Na^+ tail currents after repolarization were measured using a two-pulse protocol, from −100 mV. The first pulse was applied to activate Na^+ conductance maximally (1·5 ms depolarization to 5 mV, Fig. 6*A*), followed by a second pulse to repolarize the membrane to more negative potentials, ranging from −140 to −40 mV. The second pulse induced a tail current. Figure 6*Aa* shows averaged tail current records ($n = 10$) at various repolarization potentials. The amplitude of tail current decreased and the tail current decay slowed at progressively less negative repolarization potentials. The tail current decays at the lower range of repolarization potentials (−130 to −95 mV) were fitted by a double-exponential function, while those in the less negative voltage range by a mono-exponential function (eqns (1) and (2)).

Figure 6*Aa* is a plot of the amplitude of the fast component of the tail current against the repolarization potential. The plot of the tail current amplitudes produced by the second pulse against the repolarization potential gives the instantaneous behaviour of Na^+ channels. The instantaneous *I–V* relationship was clearly sigmoidal, fitted by the logistic growth model curve (eqn (5); V_h, −87 mV; k,

---

inactivation. A repetitive depolarizing ten-pulse train to −40 mV (V_t; pulse duration, 40 ms) from a holding potential (V_h) of −90 mV was applied. *a*, averaged peak Na^+ current records ($n = 5$) at four different pulse numbers (frequency, 10 Hz). *b*, plot of family of curves of normalized Na^+ current against the indicated pulse numbers in the train at the different frequencies indicated on the right. The normalization was done relative to the amplitude of Na^+ current produced by the first pulse at a particular frequency. Note the gradual drop in the current amplitude with increasing pulse number and saturation of the current to achieve the equilibrated state. Arrows indicate the pulse numbers at which the averaged Na^+ current records are illustrated in *a*. *c*, plot of the normalized fraction of Na^+ current at the equilibrated state determined from the plot in *B* against the interpulse interval of the stimulation frequency. With the assumption that most of the Na^+ current recovery occurs during the interpulse interval, it can be estimated that a recovery interval of about 1 s is required for the Na^+ channels to attain a 95% recovery from the inactivated state.

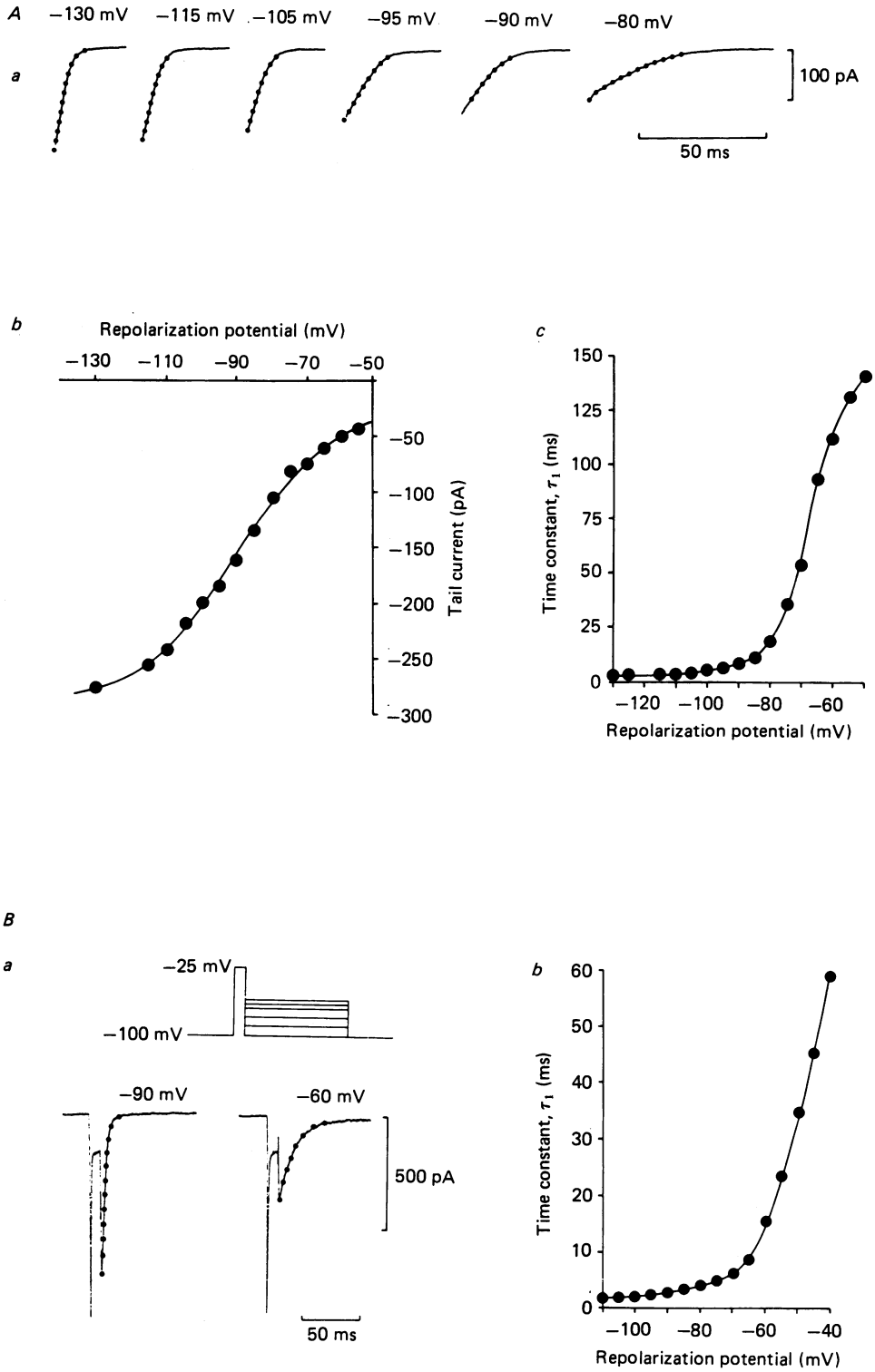

Fig. 6. For legend see opposite.

14·3 mV). Such a deviation from the normal ohmic relationship was found to be a reproducible feature of these cells ($n = 5$).

The time constants (τ_1) derived from the exponential fits of the tail current records, i.e. the value estimated from the single-exponential fit and the value of the fast component estimated from the double-exponential fit were plotted against the repolarization potential (Fig. 6*Ac*). The time constant decreased in a non-linear fashion from 141 ms at −55 mV to 2·2 ms at −130 mV, with the largest departure from linearity centred on −80 mV.

Figure 6*B* shows tail current kinetics using slightly different parameters for the first pulse (pulse duration, 10 ms; membrane potential (V_m), −25 mV). Observations were similar to those described for Fig. 6*A*; tail currents at negative repolarizations (−115 to −90 mV) were best fitted by a double-exponential function. An abrupt change of slope in the plot of τ_1 against repolarization occurred in the vicinity of −70 mV (Fig. 6*Bb*). This might be related to the uncertainty in separating the two components in this region (Schauf, Bullock & Pencek, 1977).

Power spectrum from non-stationary sodium current fluctuations

At low depolarizing steps (V_m = −70 to −40 mV), I_{Na} activated and inactivated slowly, and the opening and closing of Na^+ channels were seen as fluctuations in the current trace. The kinetics of activation and inactivation of Na^+ channels were determined from non-stationary I_{Na} fluctuations computed using the method of Conti, Neumcke, Nonner & Stampfli (1980) and Sigworth (1984). The drift in the

Fig. 6. *A*, characteristics of Na^+ tail current at different repolarization potentials. *a*, family of averaged Na^+ tail currents ($n = 10$) at different repolarization potentials. After a 1·5 ms pulse to +5 mV from a holding potential of −100 mV, the membrane was repolarized to the potentials indicated above the traces. The dots superimposed on the tail current traces represent the fit of the tail current decays by either a double- or a single-exponential function (eqns (1) and (2) in text). The initial 1·2 ms of the tail current records contaminated by capacitive transients were discarded for estimations of exponential fits. *b*, instantaneous *I–V* curve. Plot of tail current amplitudes determined by extrapolation of the tail currents to the end of the pre-pulse against the repolarization potential. The amplitudes of the fast component derived from the double-exponential fit and the amplitudes of tail currents derived from single-exponential fit plotted against the membrane potential. The instantaneous *I–V* relationship is sigmoidal and the line was drawn through the data points using the logistic growth curve model (eqn (5) in the text, with V_h = −89 mV, k, the slope factor = 14·3 mV). *c*, voltage dependence of the time constant of the tail current decay of the fast component (τ_1). Pooled data of time constants of the fast component derived from the double-exponential and single-exponential fits plotted against the repolarization potential. Note the sharp inflexion in the curve at around −80 mV. *B*, characteristics of Na^+ tail current decays following a depolarizing pre-pulse of long duration (10 ms). *a*, family of averaged peak Na^+ currents ($n = 10$) generated by a constant pre-pulse to −25 mV from a holding potential of −100 mV, followed by tail currents produced by repolarizing the membrane to potentials indicated above the traces. The dots overlapping the tail currents signify single- or double-exponential fits to the tail current decays (eqns (1) and (2)). Capacitive transients were eliminated by discarding the initial 1·2 ms of the tail current decays. *b*, voltage dependence of tail current decays. The decay time constant of the fast component derived from the double- and single-exponential fits (τ_1) are plotted against the membrane potential. Note departure from monotonic decay of the time constant values around −70 mV.

baseline due to the inactivation characteristics of I_{Na} was removed by subtracting the mean from individual currents.

Figure 7 shows individual (*A*) and averaged (*B*) I_{Na} traces, and samples of I_{Na} fluctuations derived from individual records after subtraction of the mean I_{Na} (*C*). Figure 7*D* is the power spectrum obtained by averaging the fluctuations illustrated in 7*C*. A single Lorentzian function (eqn (3)) adequately fitted the power spectrum. Figure 7 *A–D* was obtained using a test pulse to −70 mV. The time constant derived from the Lorentzian fit at −70 mV was faster (0·44 ms) than the value obtained for I_{Na} fluctuations at a more depolarized potential (1·06 ms, −60 mV, Fig. 7*E–H*).

Variance of sodium current fluctuations and single-channel conductance

We obtained an estimate of the single-Na^+-channel conductance (γ_{Na}) from fluctuation analysis in voltage clamped gonadotrophs under conditions where I_{Na} was reduced by a depolarizing pre-pulse (for review see Neher & Stevens, 1977). Reduction in I_{Na} does not significantly affect the estimated value of γ_{Na} (Sigworth, 1980) and fluctuations at the beginning or end of the pulse give comparable values (Neumcke & Stampfli, 1982). Figure 8*A* and *B* illustrates the ensemble variance and mean current, respectively, calculated by depolarizing the membrane to −20 mV, following a pre-pulse to −38 mV, from a holding potential of −100 mV.

Both the variance and mean current showed a time-dependent parallel decrease. Slow inactivation of the inward current might be an important factor contributing to the observation of a systematic drift (Adelman & Palti, 1969; Conti *et al.* 1980). The parallel decline in the mean current and variance, however, indicates that the slow inactivation step does not affect channel conductance, assuming there is only a single level of conductance from a closed state. The time-dependent changes in the current and variance may be interpreted by assuming that I_{Na} is the sum of unitary currents which flow through N homogenous, independent channels with only one level of conductance. Assuming that the probability of the channel in the open state at time t after depolarization pulse is described by the stochastic parameter $p(t)$, then the time course of the mean current, $I_{Na}(t)$, and the variance, $\sigma^2_{Na}(t)$, can be described by:

$$I_{Na}(t) = iNp(t) \tag{6}$$

$$\sigma^2_{Na}(t) = i^2Np(t)\,[1-p(t)], \tag{7}$$

where i is the current through a single Na^+ channel and N is the total number of channels.

Figure 8*C* is a plot of variance against the mean current. Note from the scatter plot that the variance value is high when the current amplitude is high, which indicates that the amplitude of Na^+ current fluctuations is related to the amplitude of the mean current. One would expect a parabolic relationship at higher current magnitudes since the fluctuations would flatten as a result of maximal channel opening.

From eqns (6) and (7), it is possible to derive the following equation:

$$\sigma^2_{Na}(t)/I_{Na}(t) = i[1-p(t)], \tag{8}$$

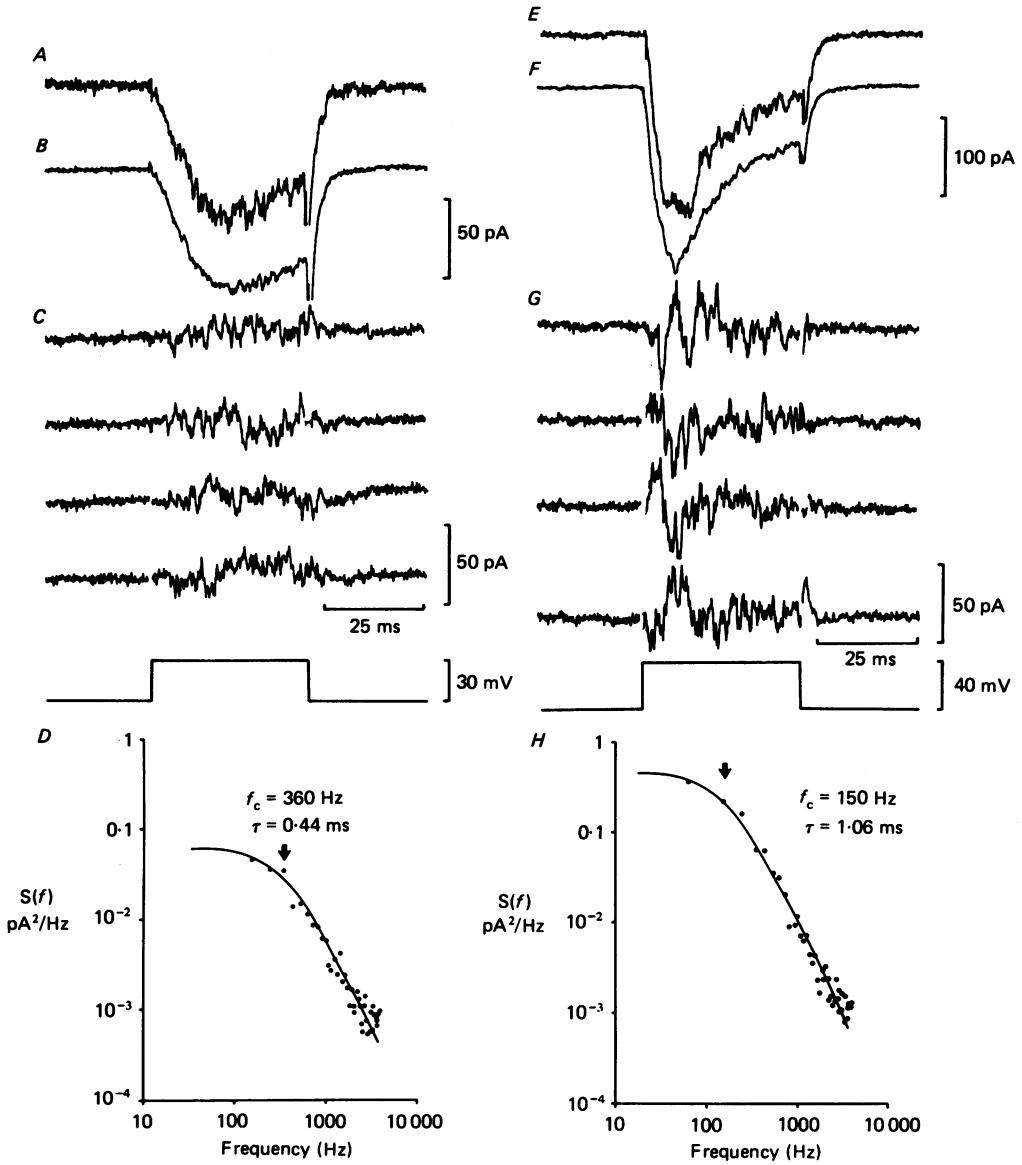

Fig. 7. Non-stationary Na^+ current fluctuations and power spectra from records of Na^+ current at two different membrane potentials. *A–D*, at −70 mV and *E–H* at −60 mV; holding potential = −100 mV. *A* and *E*, single Na^+ current traces. *B* and *F*, averaged Na^+ current record (n = 11). *C* and *G*, set of residual Na^+ current fluctuation records after subtraction of the mean current from individual Na^+ current traces. *D* and *H*, power spectra constructed from the residual Na^+ current fluctuations. The line describes the single Lorentzian fit to the data points (eqn (3) in text). Note the time constant derived from the corner frequency value (f_c) estimated from the single Lorentzian fit is faster (0·44 ms) at −70 mV (*D*), while it is slower at −60 mV (1·06 ms, *F*).

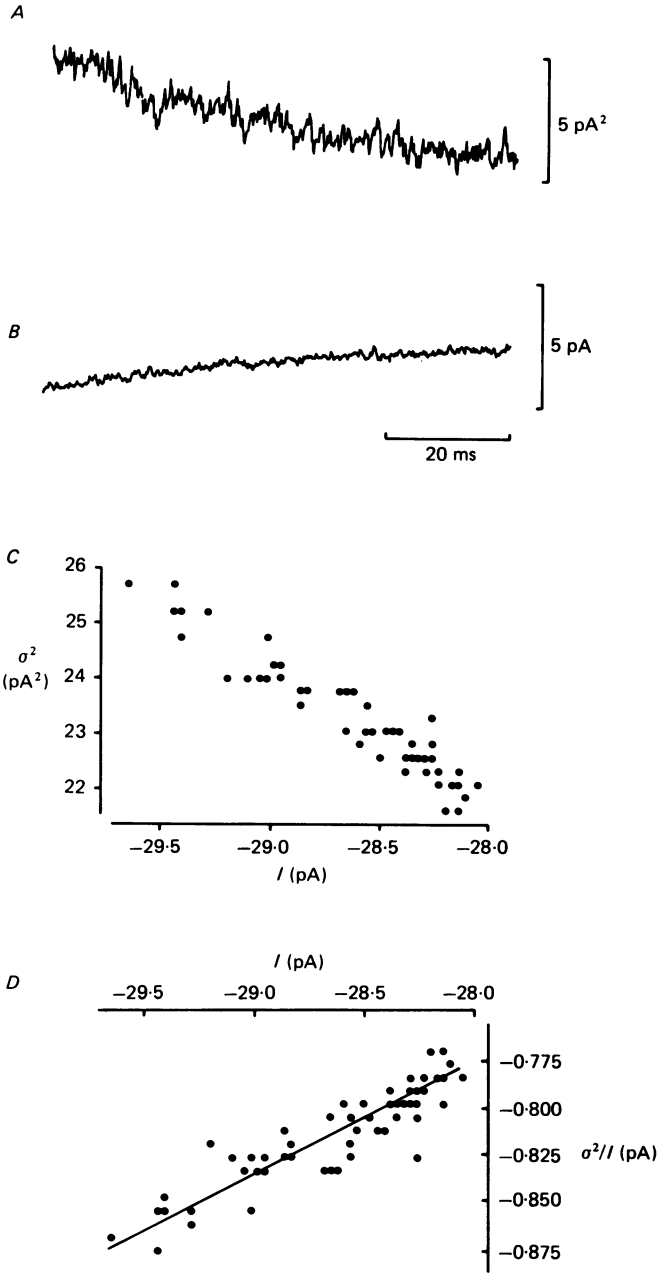

Fig. 8. Variance and mean Na^+ current calculated from an ensemble of Na^+ current traces obtained by 100 ms depolarization step to −20 mV, following a pre-pulse to −38 mV of 80 ms duration. Time course of the variance (σ^2, *A*) and the mean Na^+ current (*B*). Records between 5 and 85 ms are illustrated. *C*, scatter plot of isochronal variance (σ^2) against the mean Na^+ current (*I*). *D*, plot of the ratio (σ^2/I) against the mean Na^+ current, *I*. The straight line was drawn according to the linear regression eqn (9) in the text. The regression coefficient was 0·91. The *Y*-intercept determined from the linear regression fit was 0·8 pA.

which by rearrangement using eqn (6) yields:

$$\sigma^2_{Na}(t)/I_{Na}(t) = i - I_{Na}(t)/N. \quad (9)$$

Equations (8) and (9) are of linear regression form, showing the derivation of both the single-channel current (i) and the number of channels (N) without knowing the value of $p(t)$. Therefore when σ^2_{Na}/I_{Na} is plotted against the mean current (I_{Na}), the y-intercept of the regression line gives the unitary current value (i). Figure 8*D* is a relation of σ^2_{Na}/I_{Na} *versus* I_{Na} obtained from isochronal σ^2_{Na} and I_{Na} values shown in Fig. 8 *A* and *B*, respectively. A unitary current value of 0·8 pA was estimated from

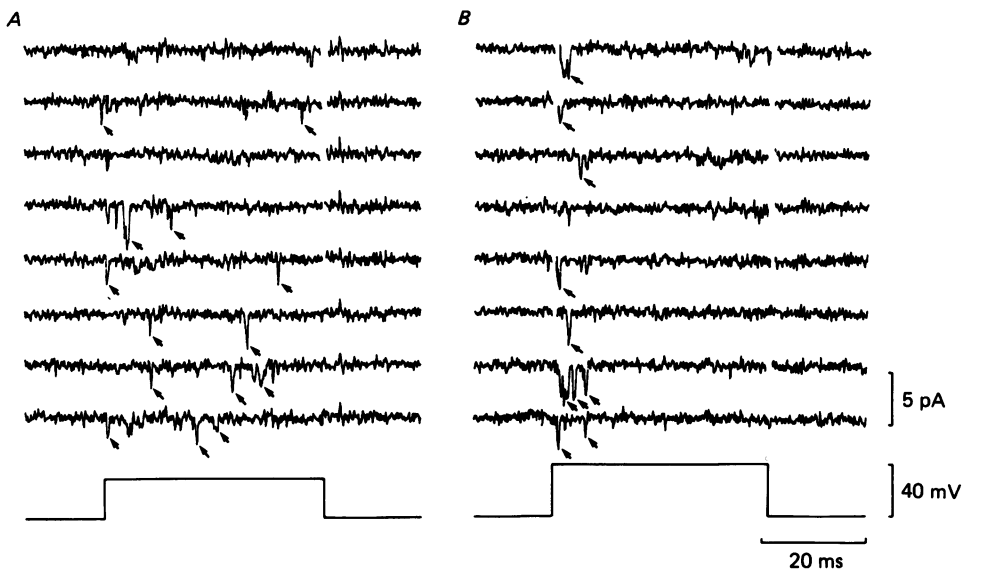

Fig. 9. Patch clamp (outside-out) recordings illustrating the time course of the appearance of the single Na^+ channel currents following a 40 ms depolarization to −70 (*A*) and −60 mV (*B*). The arrows point at the single-channel currents. Note that the occurrence of the single-channel currents was randomly distributed during the duration of the pulse at −70 mV, while they were concentrated at the beginning of the pulse at a slightly higher membrane potential of −60 mV. The patch pipette contained Cs^+ solution (Table 1). Holding potential, −100 mV, low-pass filter, 2 kHz.

the linear regression fit. From the single-channel current (i) and the theoretical Na^+ equilibrium potential, (E_{Na}) of 82 mV, a chord conductance ($\gamma_{Na} = i/E - E_{Na}$) of 8 pS was estimated for this cell (mean ± S.D. = 10·3 ± 3, n = 3). The γ_{Na} estimate is close to the previously reported values in other preparations (Conti *et al.* 1980; Sigworth, 1980; Ohmori, 1981; Neumcke & Stampfli, 1982).

Single-sodium-channel currents

To relate the kinetics of Na^+ channels analysed using stationary and non-stationary I_{Na} fluctuations to the behaviour of single Na^+ channels we performed outside-out patch recordings. The appearance of single-Na^+-channel currents was widespread in the time during the duration of the pulse application (Fig. 9*A*,

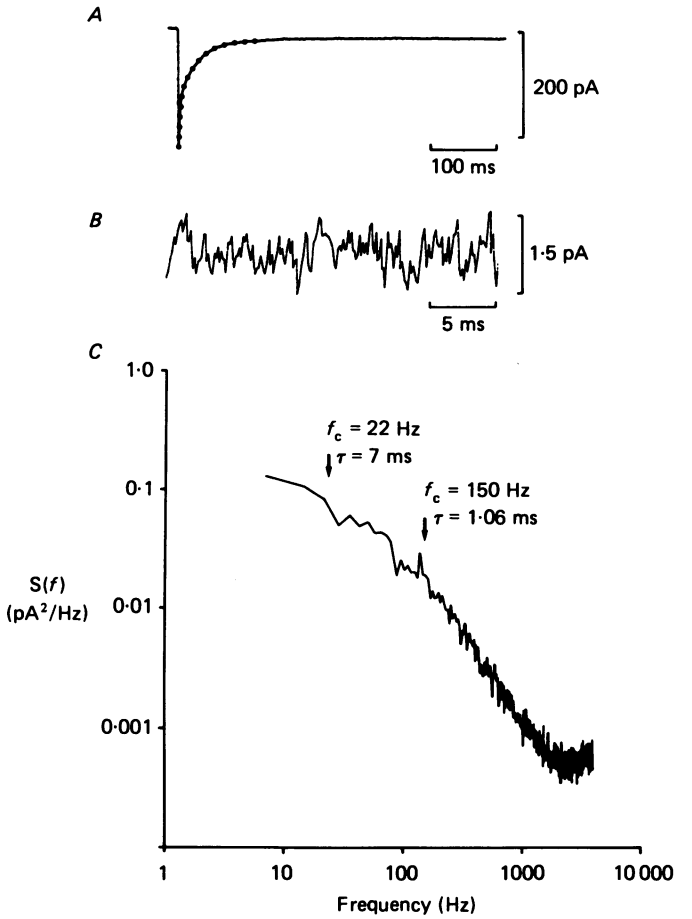

Fig. 10. Modification of Na^+ channels by 15 mM-internal iodate. *A*, activation followed by slow inactivation of Na^+ current produced by 600 ms depolarization to −32 mV, with 15 mM-iodate in the pipette. The Na^+ current record is an average of seventy-six current traces. The inactivation phase was fitted by a double-exponential function (indicated by superimposed dots, eqn (2) in the text). *B*, sample of Na^+ current fluctuation record extracted from the steady-state portion of the Na^+ current depicted in *A*. *C*, spectral density of Na^+ current fluctuations obtained from the steady-state region of the mean Na^+ current record shown in *A*. Arrows indicate corner frequencies (f_c) and the time constants (τ) of the underlying fluctuations determined from the double Lorentzian fit (eqn (4) in the text).

membrane potential, −70 mV), while at a slightly more depolarized potential (−60 mV, Fig. 9*B*) the single-Na^+-channel currents occurred at the pulse onset. The single-channel-current size of about 1·5 pA is close to the values reported for muscle cells (Sigworth & Neher, 1980), bovine chromaffin cell (Fenwick, Marty & Neher, 1982) and rat clonal pituitary A/GH3 cell (Fernandez, Fox & Krasne, 1984) although it is slightly greater than the value of single-channel current estimated from fluctuation analysis (Fig. 8).

Modification of sodium current inactivation by internal iodate

The activation and inactivation phases of I_{Na} form part of a complex gating reaction, with transitions occurring from one state to the other; the inactivation process may also proceed with complex kinetics involving transitions through two or more substates. Information on the molecular basis of these gating processes can be obtained by using agents which modify their kinetics. Internal application of iodate, for example, modifies inactivation of I_{Na} although it does not affect the activation phase (Stampfli, 1974; Neumcke, Schwartz & Stampfli, 1980; Schmidtmayer, Stoye-Herzog & Ulbricht, 1983).

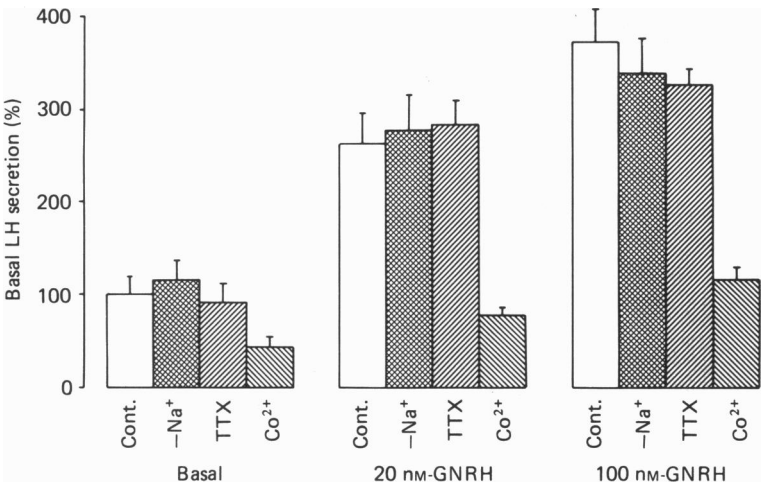

Fig. 11. Role of Na^+ channels in gonadotrophin secretion. Note that the basal and GNRH-induced LH release was not affected by absence of Na^+ in the medium nor was it affected by blocking the Na^+ channels with tetrodotoxin (TTX, 30 μM). Blocking the Ca^{2+} channels with Co^{2+} (2 mM) however, attenuated LH release. Cont., control.

Figure 10 illustrates results in which the gonadotroph Na^+ channels were modified by dialysing the cells with 15 mM-sodium iodate (IO_3^- soln, Table 1). A prominent increase in the inactivation time course of I_{Na} is clearly evident from the averaged record obtained by using a voltage pulse from -100 to -32 mV. The inactivation phase of I_{Na} was described by a double-exponential function (eqn (2)).

Using iodate in kinetic studies of Na^+ channels enhances the underlying fluctuations due to random opening and closure of Na^+ channels (Neumcke *et al.* 1980). Figure 10*B* illustrates the fluctuations in I_{Na} in the steady-state region of the record shown in *A*, while *C* is the power density spectrum computed from these fluctuations. The spectral density was fitted by a double Lorentzian function (eqn (4)). The time constant of the fast and slow processes was estimated to be 1·1 ms (f_c = 150 Hz) and 7 ms (f_c = 22 Hz), respectively. Both time constants could be related solely to the inactivation phenomenon: the arguments in favour of this are evidence from non-stationary current fluctuations and single-channel data in gonadotrophs.

Sodium channel involvement in the secretion of luteinizing hormone

In order to examine the functional role of voltage-gated Na^+ channels in LH secretion by the gonadotrophs, we assayed the amount of LH released in the culture medium under control conditions with Na^+ present in the medium and under conditions of Na^+ channel blockade by TTX (30 μM) or removal of extracellular Na^+. Both basal and GNRH-stimulated LH secretion were examined at two different concentrations of GNRH (20 and 100 nM): neither were significantly affected either by the absence of Na^+ in the medium or under conditions of Na^+ channel blockade by TTX (Fig. 11).

DISCUSSION

We have described the quantitative characteristics of isolated Na^+ currents (I_{Na}) in normal gonadotrophs derived from the ovine pars tuberalis. The characteristics of the isolated I_{Na} qualitatively resemble I_{Na} in cultured lactotrophs of the pituitary (Cobbett, Ingram & Mason, 1987), neoplastic pituitary cells (Fernandez *et al.* 1984; Matteson & Armstrong, 1984), neuroblastoma cells (Moolenar & Spector, 1978), and adrenal chromaffin cells (Fenwick *et al.* 1982). The gross similarities lay in the rapid activation and inactivation of I_{Na} to a steady-state value on application of a depolarizing voltage step, and in TTX sensitivity.

Gating characteristics of gonadotroph sodium current

The gating kinetics of Na^+ channels formulated by Hodgkin & Huxley (1952*a*,*b*) describe the transition between activation and inactivation states to be a first-order process. While the simple Hodgkin–Huxley scheme explains the gating kinetics of Na^+ channels in some systems, data on other membrane systems have accumulated which favour a rather more complex gating mechanism, with the activation and inactivation states being characterized by transitions occurring through a series of coupled reactions as opposed to a simple independent process.

Our observations on the kinetics of I_{Na} in gonadotrophs can be explained by the 'coupled' model. The first evidence is the substantial delay of the inactivation process, on the order of 700–900 μs (Fig. 5*A*). The delay in the activation onset can be interpreted to mean that inactivation only sets in after a channel is fully activated and corroborates previous findings (Goldman & Schauf, 1972; Bezanilla & Armstrong, 1977). The transition between activation and inactivation in the gonadotrophs, therefore, can be explained by the 'coupled' reaction model of Bezanilla & Armstrong (1977) in the following way:

$$C \rightleftharpoons O \rightleftharpoons I_1 \rightleftharpoons I_2,$$

where C is the closed state, O the open state and I_1 and I_2 are the inactivated states.

The long delay in the onset of inactivation can be interpreted to mean that current inactivation in the gonadotrophs could develop from the closed state preceding the open one (Bean, 1981), the result being a considerable delay in build-up of the inactivation state imposed by this additional gating step.

Secondly, contrary to expectations of Hodgkin–Huxley formalism which predicts an exponential recovery, the peak Na^+ channel recovery in gonadotrophs showed a sigmoidal time course with an initial delay of a few milliseconds (e.g. Fig. 5*B*). The finding is similar to that reported previously in *Myxicola* giant axons (Schauf, 1974) and in myelinated nerve from *Rana pipiens* (Chiu, 1977).

Using iodate, therefore, we confirmed the complexity in the inactivation kinetics involving two substates, one with fast and the other with slow kinetics. This again justifies a three-state model to describe the inactivation state. The two time constants estimated from double Lorentzian function fit of the power spectrum was close to the time constant values derived from the double-exponential fit (eqn (2), $\tau_1 = 0{\cdot}98$ ms, $\tau_2 = 11$ ms) of the inactivation phase in the same cells (Fig. 10*A*). Such a 'coupled' scheme, may in fact be more biologically relevant, since all transitions between gating states can be described by discrete changes in the conformation of a single-channel macromolecule.

Sodium tail currents at different repolarization potentials

Departures from the predictions of Hodgkin–Huxley formalism were also evident from the kinetics of tail current decays at different repolarization potentials. Under the Hodgkin–Huxley scheme, in the two-pulse experiments described in Fig. 6 the repolarization occurs at a point where the m variable is close to unity ($m = 1$), and the h variable is slightly less than 1 ($h < 1$). The effect of a sudden change in the potential on repolarization will be a sudden surge in inward I_{Na} due to increase in the driving force which will decay with kinetics governed by the m and h parameters. The values of m and h can be predicted to be different at the different repolarization potentials.

Two features may be distinguished. Thus at negative repolarization potentials (-100 mV or more), the steady-state values of m and h are 0 and 1 and the Na^+ channel conductance, g_{Na} (m^3h) should decrease to zero (since m changes from 1 to 0 while h remains unchanged and the tail current decay described by a mono-exponential function. On the contrary, the gonadotroph tail currents in this range were described by a double-exponential function.

Similarly, in the less negative repolarization potential range a double-exponential function composed of an initial component with a rapidly decaying event resulting from the transition of $m = 1$ before repolarization, to its equilibrium value $m = 0$, followed by a slow decay attributable to the transition of the h parameter to its equilibrium value ($h > 0$) can be predicted. Our observations were contrary to this prediction: decays with single-exponential function were the characteristic feature. This general trend in the tail current decays at the different repolarization potentials did not depend on the duration of the test pulse. Our findings on the departure from the Hodgkin–Huxley scheme therefore corroborate similar observations reported in other preparations (Schauf *et al.* 1977).

The tail currents at the end of long pulses (> 5 ms) were TTX-sensitive, and we believe that the late tail currents were due to the opening of the same Na^+ channels that gave rise to the transient I_{Na}. The delayed tail currents can be explained by the existence of a distinct population of activatable Na^+ channels during the steady state, accounted for by the failure of the steady-state activation and inactivation

parameters, m and h, to reach absolute zero value over a certain potential range (Hodgkin & Huxley, 1952*b*; Attwell, Cohen, Eisner, Ohba & Ojeda 1979). Another plausible explanation would be the existence of a second open state linked to the inactivated state (Chandler & Meves, 1970; Bezanilla & Armstrong, 1977)

Power spectra of non-stationary fluctuations of sodium current

Power spectral density plots from ensembled non-stationary I_{Na} fluctuations gave an estimate of the time constants of the Na^+ channel kinetics which indicated that the time constant at less depolarized potentials was shorter than that of fluctuations at more positive depolarizations (Fig. 7). The two different time constants can be related to the different kinetics of Na^+ channels at the two different potentials, the faster being related to activation, and the slower related to inactivation.

This is apparent from inspection of I_{Na} at the two different potentials. While the current trace indicates slow, sustained activation during the voltage pulse (Fig. 7*A*), the additional inactivating component is evident at a slightly higher depolarization (Fig. 7*E*), similar to earlier findings (Conti *et al.* 1980). From their analysis of I_{Na} fluctuations, power spectral density was found to be concentrated in two distinct frequency zones, over the high-frequency range for small depolarizations, while at larger depolarizations it lay in the low-frequency range.

Additional evidence favouring such a conclusion was obtained from single-channel data illustrated in Fig. 9. At smaller depolarizations new channels are continuously recruited into the open pool during the depolarization period, reflecting sustained activation of the channels, while at a slightly larger depolarization step the open channels are concentrated at the beginning of the pulse step and then inactivate.

Gonadotroph sodium channels and hormone secretion?

Our data suggest that Na^+ channels are not important in hormone secretion (Fig. 11). These findings essentially corroborate results previously reported (Conn & Rogers, 1980). What, then, are the implications in relation to the importance of Na^+ channels in the stimulus–secretion process, and how does such a result relate to the electrophysiological properties of gonadotrophs?

The irrelevance of gonadotroph Na^+ channels in hormone secretion can firstly be attributed to channel inactivation at rest. The voltage dependence of the inactivation process revealed a half-maximal inactivation occurring in the negative potential range of -70 mV. This is close to that observed in mammalian muscle (-70 mV, Adrian & Marshall, 1977); somatic membrane of the dorsal root ganglion (-80 mV, Kostyuk, Veselovsky & Tsyndrenko, 1981); cultured mouse neuroblastoma cells (-65 mV, Moolenar & Spector, 1978); and rabbit myelinated nerve (-55 mV, Chiu, Ritchie, Rogart & Stagg, 1979). However, the half-maximal value for the gonadotrophs is a clear departure from that reported for other normal and neoplastic endocrine cells, for example -40 mV for adrenal chromaffin cells (Fenwick *et al.* 1982), -45 mV in bovine lactotrophs (Cobbett *et al.* 1987) and -50 mV for neoplastic pituitary GH3 cells (Dubinsky & Oxford, 1984). Since the resting membrane potential of the gonadotrophs is around the half-maximal inactivation range for these cells (Mason & Waring, 1985), this would imply that only about 50% of the Na^+ channels are functionally active at rest and might account for the small

action potential size observed under current clamp (Fig. 1*A*). If the Na^+ channels are related to a depolarizing event associated with secretion, then it can be foreseen that half of the Na^+ channels would not participate. Interestingly, intracellular recordings from gonadotrophs have found that most (> 95%) do not fire spontaneously (Mason & Waring, 1985).

The second property limiting the role of Na^+ channels in hormone secretion by the gonadotrophs is the poor sustenance of regenerative Na^+ currents to repeated activation in these cells. A recovery period from inactivation of about 1 s was estimated. This property therefore questions the practical utility of gonadotroph Na^+ channels in depolarization-related gonadotrophin secretion. A substantial difference is evident when comparing these results with those in neurones. In neurones, antidromic activation of Na^+-dependent action potentials is possible using an interpulse interval of 10 ms or less. Interestingly, the observation of a long recovery period in the gonadotrophs agrees well with similar observations made in bovine lactotrophs (Cobbett *et al.* 1987), and like the gonadotrophs, lactotroph Na^+ channels do not seem to be essential for prolactin secretion.

A third possible factor can be attributed to the sigmoidal *I–V* relationship of single-Na^+-channel behaviour assessed from instantaneous currents (Fig. 6*Ab*), the effect of which would be to suppress the voltage-dependent Na^+ conductance mechanism under conditions of a linearly rising membrane depolarization.

We wish to thank Miss A. L. V. Tibbs for her excellent technical support related to this work, and Mr R. Bunting for preparing the illustrations. We are particularly grateful to the Lalor Foundation who supported Dr Sikdar, and to the Nuffield Foundation and the Burroughs Wellcome Foundation who generously supported early stages of this work in which Dr Dennis Waring was involved.

REFERENCES

ADELMAN JR, W. J. & PALTI, Y. (1969). The effects of external potassium and long duration voltage conditioning on the amplitude of sodium currents in the giant axon of the squid, *Loligo peali*. *Journal of General Physiology* **54**, 589–606.

ADRIAN, R. H. & MARSHALL, M. W. (1977). Sodium currents in mammalian muscle. *Journal of Physiology* **268**, 223–250.

AGNADO, L. I., HANCKE, J. L., RODRIGUEZ, S. & RODRIGUEZ, E. M. (1982). Changes in the luteinizing hormone content of the rat pars tuberalis during the estrus cycle and after lesions in the preoptic area. *Neuroendocrinology* **35**, 178–185.

ATTWELL, D., COHEN, I., EISNER, D., OHBA, M. & OJEDA, C. (1979). The steady-state TTX-sensitive ('window') sodium current in cardiac Purkinje fibres. *Pflügers Archiv* **379**, 137–142.

BEAN, B. P. (1981). Sodium channel inactivation in the crayfish giant axon. Must channels open before inactivating? *Biophysical Journal* **35**, 595–614.

BEZANILLA, F. & ARMSTRONG, C. M. (1977). Inactivation of the sodium channel. I. Sodium current experiments. *Journal of General Physiology* **70**, 549–566.

CHANDLER, W. K. & MEVES, H. (1970). Evidence for two types of sodium conductance in axons perfused with sodium fluoride solution. *Journal of Physiology* **211**, 653–678.

CHILDS, G. V., HYDE, C., NAOR, Z. & CATT, K. (1983). Heterogenous luteinizing hormone and follicle-stimulating hormone storage patterns in subtypes of gonadotrophs separated by centrifugal elutriation. *Endocrinology* **113**, 2120–2128.

CHIU, S. Y. (1977). Inactivation of sodium channels: second-order kinetics in myelinated nerve. *Journal of Physiology* **273**, 573–596.

CHIU, S. Y., RITCHIE, J. M., ROGART, R. B. & STAGG, D. (1979). A quantitative description of membrane currents in rabbit myelinated nerve. *Journal of Physiology* **292**, 149–166.

COBBETT, P., INGRAM, C. D. & MASON, W. T. (1987). Sodium and potassium currents involved in action potential propagation in normal bovine lactotrophs. *Journal of Physiology* **392**, 273–299.

CONN, P. M. & ROGERS, D. C. (1980). Gonadotrophin secretion from pituitary cultures following activation of endogenous ion channels. *Endocrinology* **107**, 2133–2134.

CONTI, F., NEUMCKE, B., NONNER, W. & STAMPFLI, R. (1980). Conductance fluctuations from the inactivation process of sodium channels in myelinated nerve fibres. *Journal of Physiology* **308**, 217–239.

DENEF, C., SWENNEN, L. & ANDRIES, M. (1982). Separated anterior pituitary cells and their responses to hypophysiotropic hormones. *International Review of Cytology* **76**, 225–244.

DUBINSKY, J. M. & OXFORD, G. S. (1984). Ionic currents in two strains of rat pituitary tumour cells. *Journal of General Physiology* **83**, 309–339.

FENWICK, E. M., MARTY, A. & NEHER, E. (1982). Sodium and calcium channels in bovine chromaffin cells. *Journal of Physiology* **331**, 599–635.

FERNANDEZ, J. M., FOX, A. P. & KRASNE, S. (1984). Membrane patches and whole cell membranes: A comparison of electrical properties in rat clonal pituitary (GH_3) cells. *Journal of Physiology* **356**, 565–585.

GOLDMAN, L. & SCHAUF, C. L. (1972). Inactivation of the sodium current in *Myxicola* giant axons. Evidence of coupling to the activation process. *Journal of General Physiology* **59**, 659–675.

GROSS, D. S. (1978). Effect of castration and steroid replacement on immunoreactive luteinizing hormone cells in the pars tuberalis of the rat. *Endocrinology* **103**, 585–588.

GROSS, D. S., TURGEON, J. L. & WARING, D. W. (1984). The ovine pars tuberalis: a naturally occurring source of pure gonadotropes. *Endocrinology* **114**, 2084–2091.

HAMILL, O. P., MARTY, A., NEHER, E., SAKMANN, B. & SIGWORTH, F. J. (1981). Improved patch clamp techniques for high-resolution current recording from cells and cell-free membrane patches. *Pflügers Archiv* **391**, 85–100.

HODGKIN, A. L. & HUXLEY, A. F. (1952*a*). The dual effect of membrane potential on sodium conductance in the giant axon of *Loligo*. *Journal of Physiology* **116**, 497–506.

HODGKIN, A. L. & HUXLEY, A. F. (1952*b*). A quantitative description of membrane current and its application to conduction and excitation in nerve. *Journal of Physiology* **117**, 500–554.

KIDOKORO, Y. (1976). Spontaneous calcium action potentials in a clonal pituitary cell line and their relationship to prolactin secretion. *Nature* **258**, 741–742.

KOSTYUK, P. G., VESELOVSKY, S. & TSYNDRENKO, A. Y. (1981). Ionic currents in the somatic membrane of rat dorsal root ganglion neurones. I. Sodium currents. *Neuroscience* **6**, 2423–2430.

LAMB, T. D. (1983). 'ANADISK', a disk recorder for analogue signals. *Journal of Physiology* **343**, 16–17*P*.

MASON, W. T. & WARING, D. W. (1985). Electrophysiological recordings from gonadotrophs. Evidence for Ca^{2+} channels mediated by Gonadotrophin-Releasing Hormone. *Neuroendocrinology* **41**, 258–268.

MASON, W. T. & WARING, D. W. (1986). Patch clamp recordings of single ion channel activation by Gonadotrophin-Releasing Hormone in ovine pituitary gonadotrophs. *Neuroendocrinology* **43**, 205–219.

MASON, W. T., SIKDAR, S. K. & WARING, D. W. (1986). Voltage-dependent ionic currents in normal gonadotrophs of the ovine pars tuberalis. *Journal of Physiology* **376**, 26*P*.

MATTESON, D. R. & ARMSTRONG, C. M. (1984). Na and Ca channels in a transformed line of anterior pituitary cells. *Journal of General Physiology* **83**, 371–394.

MOOLENAR, W. H. & SPECTOR, I. (1978). Ionic currents in cultured mouse neuroblastoma cells under voltage clamp conditions. *Journal of Physiology* **278**, 265–286.

NEHER, E. & STEVENS, C. F. (1977). Conductance fluctuations and ionic pores in membranes. *Annual Review of Biophysics and Bioengineering* **6**, 345–381.

NEUMCKE, B., SCHWARZ, W. & STAMPFLI, R. (1980). Modification of sodium inactivation in myelinated nerve by *Anemonia* (U.D.) toxin II and iodate, Analysis of current fluctuations and current relaxations. *Biochemica et biophysica acta* **600**, 456–466.

NEUMCKE, B. & STAMPFLI, R. (1982). Sodium currents and sodium-current fluctuations in rat myelinated nerve fibres. *Journal of Physiology* **329**, 163–184.

OHMORI, H. (1981). Unitary current through sodium channel and anomalous rectifier channel estimated from transient current noise in the tunicate egg. *Journal of Physiology* **311**, 289–305.

SCHAUF, C. L. (1974). Sodium currents in *Myxicola* axons. Non-exponential recovery from the inactive state. *Biophysical Journal* **14**, 151–154.

SCHAUF, C. L., BULLOCK, J. O. & PENCEK, T. L. (1977). Characteristics of sodium tail currents in *Myxicola* (U.D.) axons. Comparison with membrane asymmetry currents. *Biophysical Journal* **19**, 7–28.

SCHMIDTMAYER, J., STOYE-HERZOG, M. & ULBRICHT, W. (1983). Combined action of intraaxonal iodate and external sea anemone toxin ATX II on sodium channel inactivation of frog nerve fibres. *Pflügers Archiv* **398**, 204–209.

SIGWORTH, F. J. (1980). The conductance of sodium channels under conditions of reduced current at the node of Ranvier. *Journal of Physiology* **307**, 131–142.

SIGWORTH, F. J. (1984). Nonstationary noise analysis of membrane currents. In *Membranes, Channels and Noise*, ed. EISENBERG, R. S., FRANK, M. & STEVENS, C. F., pp. 21–48. New York: Plenum.

SIGWORTH, F. J. & NEHER, E. (1980). Single Na channel currents observed in cultured rat muscle cells. *Nature* **287**, 447–449.

STAMPFLI, R. (1974). Intraxonal iodate inhibits sodium inactivation. *Experientia* **30**, 505–508.

TARASKEVICH, P. S. & DOUGLAS, W. W. (1977). Action potentials occur in cells of the normal pituitary gland and are stimulated by the hypophysiotropic peptide thyrotropin-releasing hormone. *Proceedings of the National Academy of Sciences of the U.S.A.* **74**, 4064–4067.